RESEARCH ARTICLE

3D CACT-assisted Radiofrequency Ablation Following Transarterial Chemoembolization for Hepatocellular Carcinoma: Early Experience

De-Chao Jiao, Xin-Wei Han*, Gang Wu, Jian-Zhuang Ren

Abstract

Background: To explored the value of 3D C-arm CT (CACT) guidance system in performing radiofrequency ablation (RFA) following transarterial chemoembolizationon (TACE) for hepatocellular carcinomas. Materials and Methods: RFA of hepatocellular carcinomas (HCC) were performed on 15 patients (21 lesions) with the assistance of CACT guidance system. Technical success, procedure time, complications and patient radiation exposure were investigated. The puncture performance level was evaluated on a five-point scale (5-1: excellent-poor). Complete ablation rate was evaluated after two months follow-up using enhanced CT scans. Results: The technical success rate of RFA procedure under CACT navigation system was 100 %. Mean total procedure time was 24.24 ± 6.53 min, resulting in a mean effective exposure dose of 15.4 ± 5.1 mSv. The mean puncture performance level rated for CACT guided RFA procedure was 4.87 ± 0.35. Complete ablation (CA) was achieved in 20 (95.2%) of the treated 21 tumors after the first RFA session. None of patients developed intra-procedural complications. Conclusions: 3D CACT guidance system enables reliable and efficient needle positioning by providing real-time intraoperative guidance for performing RFA on HCCs.

Keywords: Flat detector C - arm CT - Hepatocellular carcinoma - Interventional radiology - radiofrequency ablation

Asian Pac J Cancer Prev, **16 (17)**, 7897-7903

Introduction

Tumor ablation outcomes rely on three key factors: adequate visualization of the tumor for ablation planning, real-time localization of ablation probe in relation to tumor, and real-time monitoring of the ablation zone (Cho et al.,2011). Many tumors are not visible with ultrasound or become obscured during the ablation by the transient hyperechogenic zone (Wood et al.,2010). Computed tomography (CT) does not offer real-time guidance unless CT fluoroscopy is employed, resulting in increased radiation to patients and operators.

Nowadays, flat detector (FD) equipped angiographic CACT systems can be used to acquire CT-like cross-sectional images directly within the interventional suite (Kalender et al., 2007; Racadio et al., 2007; Jiao et al., 2014). Along with the development of CACT, a novel technique for RFA procedures guidance recently emerged. It offers real time visualization of RFA procedures and more flexibility in the orientation of the detector system around patient compared to traditional CT system. Therefore, the RFA procedures assisted with the advanced 3D needle guidance system can be performed in a sterile workspace with flexible system angulation capability as well as instantaneous fluoroscopic feedbacks (Rotolo et al., 2015). This technique offers high spatial resolution of less than 1 mm, as well as contrast resolution of 5 HU, which is adequate for HCC after treatment of transarterial Chemoembolization (soft tissue against very high density iodized oil). This study explored the value of flat detector CACT-guidance system in performing RFA on HCC in clinical practice.

Materials and Methods

Patients

15 consecutive patients (9 males, 6 females; mean age ,63.0±9.1 years; age range, 45-84 years) with pathology or typical imaging confirmed were enrolled in this study at the department of interventional radiology, The First Affiliated Hospital of Zhengzhou University between November 2011 and November 2013. The lesion size was recorded as the maximum diameter in the image data by one interventional radiologist (Han XW, 15 years of experience in image guided hepatic ablation). The averaged diameter of lesions was 3.35±1.20 cm, ranging from 1.25 cm to 5.00 cm. This study had been approved by hospital ethic committee. The inclusion criteria were as follows: (1) HCC diagnosis based on the increased serum alpha-fetoprotein level (>20 ng/mL) and positive imaging findings (on at least two imaging modalities); (2) no evidence of portal vein or other venous thrombosis,

*Department of Interventional Radiology, the First Affiliated Hospital of Zhengzhou University , Zhengzhou, China *For correspondence: 13592583911@163.com*

extrahepatic metastasis, or uncontrollable ascites; (4) Child-Pugh liver function class A or B; (5) the number of lesions in the liver ≤ 3. (6) adequate hepatic function (serum albumin >2.0 g/dL and total bilirubin <3 mg/dL); and (7) adequate renal function (serum creatinine <1.5 times the upper limit of the normal range).

Treatment procedures

TACE: All patients were initially treated with TACE. Hepatic artery angiography was performed using the Seldinger technique. Femoral arterial catheterization was conducted through the common hepatic artery or proper hepatic artery, and the location, number, size, and blood supply of the tumors were evaluated. Subsequently, a microcatheter was super-selectively inserted into the hepatic segmental artery branch, and then injected a mixture of iodized oil 5-15 ml (Lipiodol; Guerbet, Aulnay-sous-Bois, France) and doxorubicin 10-20 mg (Main Luck Pharmaceuticals Inc. Shenzhen, China) until the mixture entered the intrahepatic branch of the portal vein (Figure 1-b). Finally, 350-560 μm gelatin sponge particles (Main Lucky Pharmaceutical Technology Co. Ltd., Shenzhen, China) were infused to embolize the artery until the arterial blood low supplying the tumor was completely blocked (Figure 1-c). After TACE treatment, liver protection, anti-inflammatory and sedation therapies were prescribed. The interventional procedures were performed by two of this study's authors (Wu G and Jiao DC), who had 10 and 6 years of experience with this procedure, respectively.

Flat detector CACT-guidance system

Image acquisition: As the first step, 3D CACT images of the patients were acquired with a rotational angiographic system (Artis Zeego, 30 × 40 cm FD detector, Siemens Healthcare, Germany). During the image acquisition, the region of interest was positioned in the isocenter and the C-arm rotated 200 degree in 8 seconds. As an output, a total number of 397 projection images were generated with an X-ray dose of 0.36 μGy/frame, projection increment 0.5°, 1-k matrix, zoom factor 0, and field of view 480 mm. With the detector used, the imaged volume covered had a cylindrical shape with a height of 185 mm, a diameter of 225 mm and a voxel size of 0.4 mm. The patients held their breaths for the entire 8 seconds 3D CACT image acquisition. The resulting raw projection images were then automatically transferred to a workstation (syngo X Workplace, Siemens Healthcare, Germany) for 3D volume reconstruction. As a result, the CACT images were reconstructed with 5 mm thickness and presented in axial, sagittal and coronal orientations. The time from the end of the data acquisition to the presentation of multiplanar images on the workstation ranged between 43 s to 45 s.

Needle path planning and guidance procedure: Image acquisition: As the second step, the needle path was planned on the same workstation using commercially available software (syngo iGuide, Siemens Healthcare, Germany). Figure 2-4 demonstrated this procedure for a 1.58 cm HCC. Figure 5-7 demonstrated this procedure for a 3.0 cm HCC. The reconstructed 3D volume was loaded first. In the orthogonal multiplanar images, the skin entry point and target lesion positions were manually selected and marked by a cross and a circle, respectively. A virtual path was then generated with its angulations and length calculated and displayed. All three multiplanar images were automatically aligned to the defined path to provide in-plane views (Figure 2 and Figure 5). This procedure could be iteratively performed, modified and reviewed until a satisfying path was obtained.

In order to use the planned path to align the needle in actual 3D space, the virtual path was then projected and superimposed onto the live fluoroscopic images and displayed on a dedicated live monitor (Figure 3 and Figure 6). The software automatically calculated the C-arm angulations, table motion, image zoom, and then controlled the C-arm moving to reach the desired position. First, the C-arm rotated to the Bull's Eye View, where the C-arm was angulated in the way that the cross and the circle displayed on live monitor completely matched and the central X-ray beam was aligned with the planned path. Thus, the skin entry point could be determined. The needle orientation was adjusted until both the tip and hub of the needle in the fluoroscopic image were superimposed and located at the center of the circle and the cross. Second, after the skin entry point and needle orientation were determined, the needle was advanced under fluoroscopy until the planned target lesion position was reached. The C-arm was rotated back and forth to two different angles subsequently to monitor the needle progression. These two angles provided lateral views (Progression View) of the planned needle path and helped to ensure that the needle was advanced along it (Figure 3 and Figure 6). Third, a 3D scan was acquired to confirm the final position of the needle (Figure 4 and Figure 7).

RFA

RFA was performed 3-7 days after TACE. All procedures were performed by an interventional radiologist (Han XW, 15 years of experience in image guided hepatic ablation) in a strictly sterile environment under general anesthesia. Once the patients were intubated, they were fixed with constraint to minimize patient movement during the procedure. In order to optimise needle placements, the baseline CT, verification of needle placement and post-procedure CT were performed at end expiration with the airway disconnected from the ventilator. Additionally, to minimize liver excursion between the end expiration (when needle placement was carried out) and the inspiration, the tidal volumes were set at low with high respiratory rate and high O_2 level. Further, to ensure that spontaneous breathing of the patient would not affect the end expiratory phase, we used muscle relaxants regularly. Otherwise the loss of muscle paralysis would impair the end tidal volume and place the liver at a much lower level.

The puncture site and pathway were determined under the guidance of CACT 3D-navigation system. RFA was performed using a 15-gauge, 9-hook expandable electrode needles (StarBurst XL, Model 1500X; Angio Dynamics, Queensbury, NY, USA) for tumor size ≥2.5 cm, and 17-gauge monopolar radiofrequency ablation needle (Cool-tip RFA system, Valleylab, Boulder, CO, USA) for tumor size <2.5 cm. Two large dispersive electrodes (ground pads) placed on the patient's thighs.

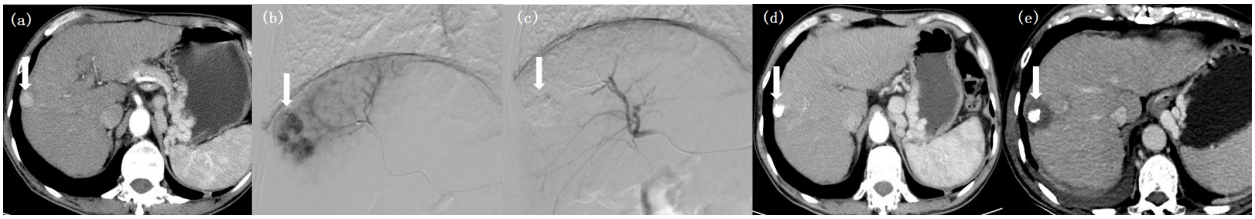

Figure 1. A 65-year-old Female with HCC (maximum diameter, 1.58 cm) in Right Lobe of the Liver. Axial image of contrast-enhanced CT before treatment, showing a high-attenuation area (arrow) (a). Selective angiography of the anterior-superior subsegmental branch of the right hepatic artery, showing hypervascular tumor adjacent to the diaphragm (b). Transarterial chemoembolization was performed, and arterial blood supply was completely blocked (c). Enhanced CT showed excellent lipiodol deposition within the lesion after 2 weeks (d). Axial image of contrast-enhanced CT obtained 2 months after RFA, showing uniform hypoattenuation without enhancement in the ablation zone (e)

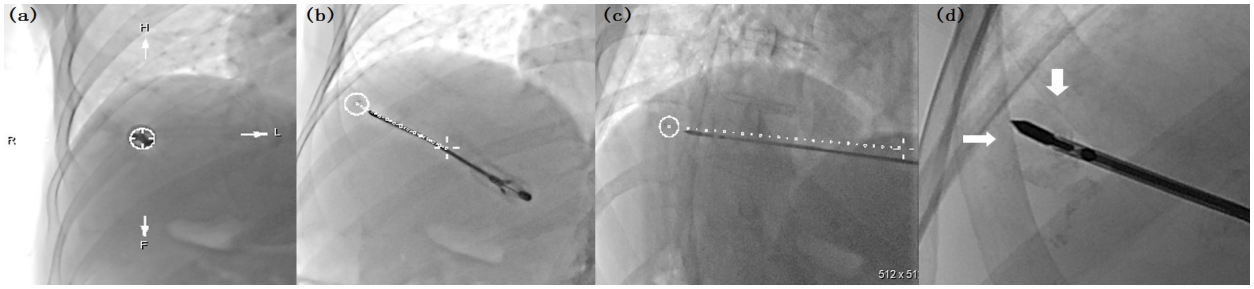

Figure 3. Real Time Fluoroscopic Images in Bull's Eye View (a) and 2 Progression Views (b-d). The needle was advanced along the planned needle path (dotted line) from skin entry site (white cross) to target lesion site (white circle)

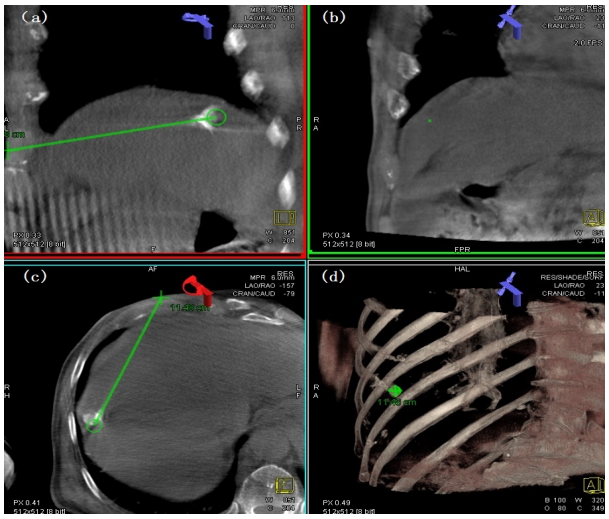

Figure 2. CACT Orthogonal Multiplanar Images With Graphics Showing Planned Needle Path (Green Line) Into Target Lesion (Green Circle). The cross indicated the skin entry site and the circle indicated the target lesion site. The needle position relative to the anatomical structures was displayed in 3D using volume rendering technique (d)

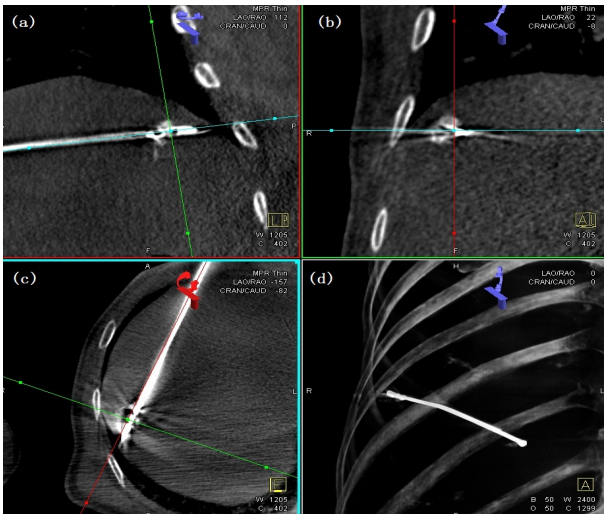

Figure 4. CACT Scan Confirmed the Needle Position in Multiplanar and Volume Rendering Images. RFA was performed using a 17-gauge monopolar radiofrequency ablation needle

The RF generator has multiple temperature displays as well as impedance and power monitoring to assist the radiologist in monitoring and controlling the ablation. The coagulation area covering the tumor focus and its surrounding area measured 5 mm or more. For tumors smaller than 2.5 cm, a single ablation was performed. For tumors larger than 2.5 cm, If CACT imaging showed that the low density of the lesions had not covered 110% of the lesions, multiple over-lapping ablations were performed. After RFA treatment, liver protection, anti-inflammatory and sedation therapies were prescribed.

Data collection and analysis

We recorded several factors during RFA: dephth of lesions from the surface, number of CT acquisitions, total procedure time (from acquisition of the initial planning CACT until the end of RFA procedure). The puncture performance level of the overall procedures was assessed by an interventional radiologist for each CACT assisted RFA on a five-point scale (5=excellent, 4=good, 3=average, 2=fair and 1=poor) (Table 1). Any complications related to the RFA were also recorded. We also recorded effective radiation exposure dose during the entire procedure (fluoroscopy dose and CBCT dose).

Follow-up

According to our follow-up protocol, Dual-phase contrast-enhanced spiral CT was done two months after treatment to evaluate local control effectiveness. At each follow-up visit, blood tests including liver function

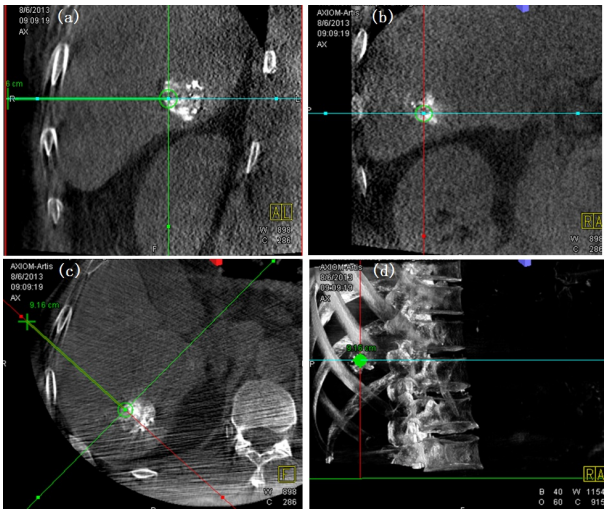

Figure 5. A 71-year-old Female with HCC (maximum diameter, 3.00 cm) in Right Lobe of the Liver. CACT orthogonal multiplanar images with graphics showing planned needle path (green line) into target lesion (green circle). The cross indicated the skin entry site and the circle indicated the target lesion site. The needle position relative to the anatomical structures was displayed in 3D using volume rendering technique

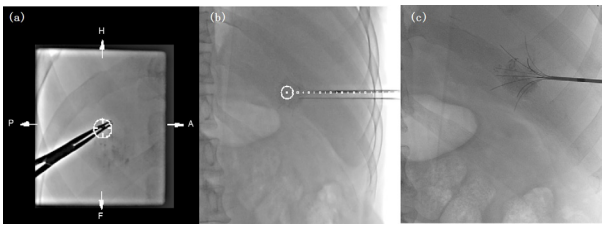

Figure 6. Real Time Fluoroscopic Images in Bull's Eye View (a) and 2 Progression Views (b-c). The needle was advanced along the planned needle path (dotted line) from skin entry site (white cross) to target lesion site (white circle)

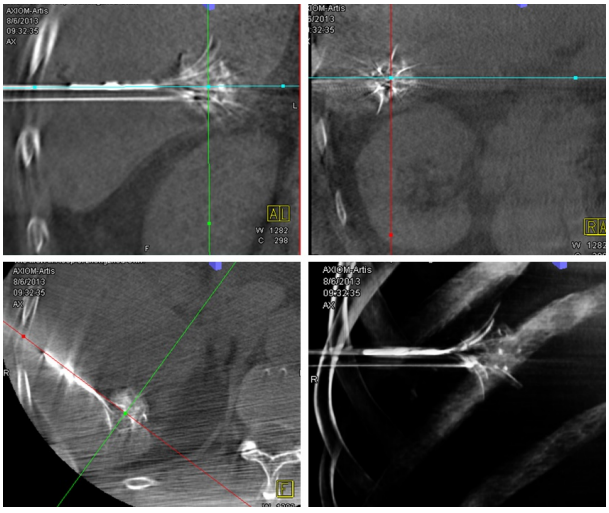

Figure 7. CACT Scan Confirmed the Needle Position in Multiplanar and Volume Rendering Images. RFA was performed using a using a 15-gauge, 9-hook expandable electrode needles

tests and serum alpha fetoprotein were done. Complete ablation (CA) was defined as uniform hypoattenuation (at CT) without enhancement in the ablation zone; for the incomplete ablated (ICA) nodules, an additional session of RFA was given with the aim of CA. All examinations were performed with spiral CT scanner (Brilliance 16, Philips, the Netherlands) by using a sequential acquisition of 5-mm-think sections, 120kV, and 250mA. Major complications were defined as complications which resulted in an admission to the hospital for therapy, an unplanned increase in the level of medical care, prolonged hospitalization or death.

Statistical analysis

All data analyses were performed using Excel 2010 (Microsoft, Redmond, WA) and SPSS software (version 13.0; SPSS, Chicago, IL). Numeric data are reported as the mean±standard deviation.

Results

Needle placement was technically successful in all 15 patients with the assistance of CACT Virtual navigation system. Readjustments of the RFA needle were necessary in 2 lesions, with single readjustment in 1 lesion and two readjustments in another lesion. The number of CACT acquisitions was 3.95±1.20. The mean puncture performance level rated for the CACT guided RFA procedure was 4.87±0.35, in which the score 5 was achieved in 19 lesions and the score 4 was achieved in the remaining 2 lesions. Complete ablation (CA) was achieved in 20 (95.2%) of the treated 21 tumors after the first session of RFA. Only one tumor closed to the major intrahepatic branches of the portal vein and inferior vena cava (size= 5 cm) was not completely ablated after the first RFA session, and incomplete ablation (ICA) was considered. This tumor was completely eradicated after second RFA procedure combined with percutaneous ethanol ablation (PEI) after two months follow-up. Mean total procedure time was 24.24±6.53 min, resulting in a mean exposure dose of 15.4 5.1 mSv. The patients' demography, treatment protocols, ablation performance, radiation dose are summarized in Table 2 and 3.

As for side effects, none of the patients developed intra-procedural complications. 8 (53.33%) patients experienced some pain after treatments, but the pain can be tolerated. 6 patients with tumor size > 4 cm, the serum alanine aminotransferase (ALT), aspartate aminotransferase (AST), and lactate dehydrogenase

Table 1. Scoring Scheme for Evaluation of the Performance Level of 3D CACT Virtual Navigation-Assisted Radiofrequency Ablation Score Criteria

Score	Criteria
5	Successful ablation No needle repositioning
4	Successful ablation 1 to 2 needle repositionings
3	Successful ablation 3 to 4 needle repositionings
2	Successful ablation More than 4 needle repositionings or reinsertion of needle is required
1	Ablation could not be completed due to needle positioning error Unsuccessful needle insertion

(LDH) levels rose transiently after treatment but returned to pretreatment levels within 1 week. In addition, 7 (46.67%) patients developed a fever after treatment, with a temperature ranging from 37.5°C to 38.8°C, which resolved without therapy within 1 week. No other clinically relevant complications, such as bleeding, subcapsular hematoma, bile duct injury, or burn injury of the skin, were noted during the follow-up period. None of the patients in this study developed local dissemination of cancer cells along the electrode puncture line.

Table 2. Lesion Characteristics and Procedure Records of CACT Guided Radiofrequency of HCC in 21 Lesions

Data collection	Value
Total No. of patient	15
Lesion diameter (cm)	3.35 ± 1.20
< 2.5 cm	5
2.50-5.00 (cm)	16
Child-Pugh grade	
A	11
B	4
AFP level	
>400 ng/ml	8
10-400 ng/ml	7
Location of the lesion	
Segment VIII	6
Segment V	4
Segment VI	4
Segment II	3
Segment IV	3
Segment VII	1
Dephth of lesions from the surface (cm)	9.11±1.79
Number of CBCT acquisition	3.95±1.20
Procedure time (min)	24.24 ± 6.53
Effevtive dose (mSv)	15.4 ± 5.1

AFP: Alpha fetal protein. CACT: C-arm computer tomography

Discussion

Guidance systems represent a major issue in image-guided percutaneous procedures, especially for frequently-moving organs. Although new systems of guidance consistent with optical, electromagnetic, or fusion imaging have been proposed to overcome such problems, their current clinical application is still limited (Hakime et al., 2012; Lee et al., 2012; Grasso et al., 2013). Due to its wide availability and the possibility of real-time guidance and intrinsic liver echogenicity, Ultrasound is the most widely used modality to guide percutaneous procedures in the liver (Wang et al., 2015). However, some cases may not be suitable for Ultrasound guidance due to tumor invisibility, high risk of collateral thermal injury, or absence of a safe electrode path (Wang et al., 2013). In such cases, CT is a valid alternative even though it may be challenging especially for "hard-to-reach" lesions (i.e., lesions of the hepatic dome, very small lesions) due to lack of real-time guidance (Hol et al., 2007).

CACT guidance is a new emerging technique incorporating both real-time fluoroscopy and CT-like imaging in the same device. This tool combines live fluoroscopic images to CACT images allowing rapid planning of needle trajectories and safe needle deployment along the planned trajectory under real-time fluoroscopy (Gupta et al., 2008).

In this study, the RFA procedures were all performed directly using a flat detector CA CT system in the interventional suite, which offered superior access to obese patients, space for needles extending outside the body, and better image support for complex, double oblique needle trajectories (Busser et al., 2013). From the results presented in this paper, the CACT based 3D needle guidance technique has been proven to effectively

Table 3. Patients Demography and Performance Evaluation of CACT Guided Radiofrequency Ablation for Hepatocellular Carcinomas (15 patients, 21 lesions)

Patient number	Gentle/Ages (years)	Diameter (cm)	Dephth of lesions from the surface	RFA treatment	Number of repositoning/ readjustment	performmance level (5-1:excellent-poor)	Outcomes
1	Male/75	4.66	8.06	RITA 1 cycle at 5 cm deployment	0	5	CA
2	Male/58	3.58	11.04	RITA 1 cycle at 5 cm deployment	0	5	CA
		4.98	7.01	RITA 2 cycles at 5 cm deployment	0	5	CA
3	Male/55	2.55	12.53	RITA 1 cycle at 5 cm deployment	0	5	CA
4	Male/84	5	8.04	RITA 2 cycles at 5 cm deployment	0	5	ICA
5	Female/71	3	9.16	RITA 1 cycle at 4 cm deployment	0	5	CA
6	Female/66	4.66	7.18	RITA 1 cycle at 5 cm deployment	0	5	CA
7	Male/62	2.56	9.32	RITA 1 cycle at 4 cm deployment	0	5	CA
		3.5	10.15	RITA 1 cycle at 5 cm deployment	0	5	CA
8	Male/45	1.68	9.08	Cool-tip single cycle 12 min	2	4	CA
9	Male/59	4.78	7.58	RITA 1 cycle at 5 cm deployment	0	5	CA
		1.25	12.56	Cool-tip single cycle 8 min	0	5	CA
		4.34	7.21	RITA 1 cycle at 5 cm deployment	0	5	CA
10	Female/65	2.04	7.93	Cool-tip single cycle 12 min	0	5	CA
		3.15	8.9	RITA 1 cycle at 4 cm deployment	0	5	CA
11	Female/57	2.76	11.55	RITA 1 cycle at 4 cm deployment	0	5	CA
		4.22	8.53	RITA 1 cycle at 5 cm deployment	1	4	CA
12	Male/59	2.4	6.87	Cool-tip single cycle 12 min	0	5	CA
13	Female/65	3.12	8.65	RITA 1 cycle at 5 cm deployment	0	5	CA
14	Female/65	1.58	11.48	Cool-tip single cycle 10 min	0	5	CA
15	Male/59	4.55	8.44	RITA 1 cycle at 5 cm deployment	0	5	CA

facilitate the needle progression procedure with puncture success rate 100%. This technique provided a reliable tool to assist RFA procedures procedure even for small lesions, and ensured high puncture success rate. For example, A lesions adjacent to the diaphragm (diameter, 1.58 cm) was punctured just once and score 5 was achieved in our study. We believe that this high puncture success rate was possible as the virtual navigation system enabled us to select a safer and more accurate targeting route in navigating the needle approach to the target during RFA procedures. Morimoto et al. (2010) treated five HCC ≤ 3 cm with percutaneous RFA under the guidance of cone-beam CT with puncture success rate of 100%. They systematically applied arterial hepatic angiography to localize the tumor. Cazzato et al. (2015) reported a similar experience in three patients with spontaneously hyperattenuating tumors. They reported a technical success in all cases, with correct needle deployment in the tumors. As for ablation performance in our study, Only one tumor closed to the major intrahepatic branches of the portal vein and inferior vena cava (size= 5.0 cm) was not completely ablated after the first RFA session, and incomplete ablation (ICA) was considered. In fact, the goal of ablation procedures is to eradicate all viable malignant cells within a designated target volume by heating the tissue to temperatures in which irreversible injury occurs (e.g. 50-54°C for 4-6 minutes (Ahmed et al., 2011). In this context, the extent of coagulation necrosis is dependent not only on the amount of energy deposited, but also on local tissue interactions and heat loss (Sun et al., 2014). Blood vessels (diameter≥3mm) abutting the target lesion prevent large temperature variations in the part of the tumor close to the vessel, thereby keeping the tissue cooler (Park et al., 2009). This so-called heat sink effect limits the effectiveness of all thermal ablation methods resulting in incomplete ablation and local tumor recurrence. Cha et al (2013) reported that RFA combined with percutaneous ethanol injection can solve the problem, especial HCCs in high risk locations.

As for side effects, none of the patients developed intra-procedural complications. 6 patients with tumor size > 4 cm, ALT and AST levels slightly rose transiently but returned to pretreatment levels within 1 week. Generally speaking, RFA only coagulates hepatic tumor, it caused limited damage to normal hepatic tissue, so it had no significant influence on hepatic function (Jiao et al., 2010). No other clinically relevant complications, such as bleeding, bile duct injury were noted after procedures.

In our study, the mean effective radiation exposure dose was 15.4±5.1 mSv, which we considered reasonable. In the study of Chiara et al (2014) that dealt with pulmonary nodules with CACT, the total dose equaled 11.62 mSv. Braak et al. (2011) reported that total mean effective doses with cone-beam CT guidance were 16.1 mSv in the upper abdomen. While, effective doses with CT-guided interventions were 20.4, and 15.4 mSv in the respective regions. On the basis of our results and the data from the literature regarding biopsies performed with CACT guidance, despite the limited amount of currently available data and the lack of homogeneity, we hypothesize that the radiation dose of CACT-guided hepatic ablation may not be a substantial problem, although a continuous effort must be made to reduce the radiation dose through use of a small field of view or collimation (mettler et al., 2008). More recently, Schegerer et al. (2014) confirmed these results but showed that they were highly dependent on CACT acquisition parameters.

A key advantage of this novel technique is that the reconstructed 3D CACT images could be acquired immediately prior to the RFA procedure. Therefore, based on the detailed anatomical information, an optimized access path for the needle insertion into the target hepatic lesion can be determined. Besides, this technique enables real time monitoring of the positioning and progression of the needle, thus any misalignment with the planned path can be corrected immediately. In addition, precise localization and documentation of the RF needle and target lesion allows clinicians to perform RFA with increased confidence, which helps to reduce the procedure and subsequent X-ray exposure time, resulting in an enhanced clinical workflow and less dose induced adverse health effects (Cheung et al., 2011).

The limitations of CACT-guided RFA should also be mentioned. The main limitation is the limited field of view compared to CT. As a result, the entire liver may not be included in the volume of acquisition. This is especially important when tumors are located in the periphery of the right liver or in obese patients. To prevent this, the CACT acquisition should be planned before the procedure and the patient should be placed in an off-center position on the table in the study (Bapst et al., 2015). Another limitation is the greater risk of motion artifacts with CACT compared to CT mostly because of slower rotation [Lee et al., 2014]. This is why we worked closely with anaesthetists in this study to optimise needle placements. It was noted that performing all procedures at the end of expiration with the airway disconnected from ventilator produced consistent positing. Additionally using lowtidal volumes with high respiratory rate and high O^2 was useful to minimise liver excursion and needle movement in the craniocaudal direction. Third limitation of the study is the small sample size (15 patients) that limits the statistical power. Future studies examining a larger population using this system are warranted.

In conclusion, CACT guidance system enables reliable and efficient needle positioning by providing real-time intraoperative guidance for performing RFA on HCCs.

Acknowledgements

This work was supported by the national high tech research and development program (863 Program) (grant number: 2015AA020301).

References

Ahmed M, Brace CL, Lee FT, et al (2011). Principles of and advances in percutaneous ablation. *Radiology*, **258**, 351-9.

Bapst B,Lagadec M, Breguet R, et al (2015). Cone Beam Computed Tomography (CBCT) in the Field of Interventional Oncology of the Liver. *Cardiovasc Intervent Radiol*.

Braak SJ, van Strijen MJ, van Es HW, et al (2011). Effective dose during needle interventions: cone-beam CT guidance

compared with conventional CT guidance. *J Vasc Interv Radiol*, **22**, 455-61.

Busser WM, Braak SJ, Futterer JJ, et al (2013). Cone beam CT guidance provides superior accuracy for complex needle paths compared with CT guidance. *Br J Radiol*, **86**, 20130310.

Cazzato RL, Buy X, Alberti N, et al (2015). Flat-panel cone-beam CT-guided radiofrequency ablation of very small (≤ 1.5 cm) liver tumors: technical note on a preliminary experience. *Cardiovasc Interv Radiol*, **38**, 206-12.

Cha D, Lee MW, Rhim H, et al (2013). Therapeutic efficacy and safety of percutaneous ethanol injection with or without combined radiofrequency ablation for hepatocellular carcinomas in high risk locations. *Korean J Radiol*, **14**, 240-7.

Cheung JY, Kim Y, Shim SS, et al (2011). Combined fluoroscopy- and CT-guided transthoracic needle biopsy using a C-arm cone-beam CT system: comparison with fluoroscopy-guided biopsy. *Korean J Radiol*, **12**, 89-96.

Chiara F, Alessandra M, Federico F, et al (2014). C-arm cone-beam computed tomography needle path overlay for percutaneous biopsy of pulmonary nodules. *Radiol Med*, **19**, 820-7.

Cho YK, Rhim H, Noh S (2011). Radiofrequency ablation versus surgical resection as primary treatment of hepatocellular carcinoma meeting the Milan criteria: a systematic review. *J Gastroenterol Hepatol*, **26**, 1354-60.

Grasso RF, Cazzato RL, Luppi G, et al (2013). Percutaneous lung biopsies: performance of an optical CT-based navigation system with a low-dose protocol. *Eur Radiol*, **23**, 3071-6.

Gupta R, Cheung AC, Bartling SH, et al (2008). Flat-panel volume CT: fundamental principles, technology, and applications. *Radiographics*, **28**, 2009-22.

Hakime A, Deschamps F, De Carvalho EG, et al (2012). Electromagnetic-tracked biopsy under ultrasound guidance: preliminary results. *Cardiovasc Intervent Radiol*, **35**, 898-905.

Hol PK (2007). Ablative therapy of liver tumors. *Acta Radiol*, **48**, 473.

Jiao D, Qian L, Zhang Y, et al (2010). Microwave ablation treatment of liver cancer with 2,450-MHz cooled-shaft antenna: an experimental and clinical study. *J Cancer Res Clin Oncol*, **136**, 1507-16.

Jiao de C, Li TF, Han XW, et al (2014). Clinical applications of the C-arm cone-beam CT-based 3D needle guidance system in performing percutaneous transthoracic needle biopsy of pulmonary lesions. *Diagn Interv Radiol*, **20**, 470-4.

Kalender WA, Kyriakou Y (2017). Flat-detector computed tomography (FD-CT). *Eur Radiol*, **17**, 2767-79.

Lee IJ, Chung JW, Yin YH, et al (2014). Cone-beam CT hepatic arteriography in chemoembolization for hepatocellular carcinoma: angiographic image quality and its determining factors. *J Vasc Interv Radiol*, **25**, 1369-79.

Lee JY, Choi BI, Chung YE, et al (2012). Clinical value of CT/MR-US fusion imaging for radiofrequency ablation of hepatic nodules. *Eur J Radiol*, **81**, 2281-9.

Mettler FA Jr, Huda W, Yoshizumi TT, et al (2008). Effective doses in radiology and diagnostic nuclear medicine: a catalog. *Radiology*, **248**, 254-63.

Morimoto M, Numata K, Kondo M, et al (2010). C-arm cone beam CT for hepatic tumor ablation under real-time 3D imaging. *Am J Roentgenol*, **194**, 452-4.

Park BK, Kim CK (2009). Complete ablation of a renal tumor abutting the inferior vena cava using a radiofrequency electrode as a lever: a case report. *Acta Radiol*, **50**, 238-240.

Racadio JM, Babic D, Homan R, et al (2007). Live 3D guidance in the interventional radiology suite. *Am J Roentgenol*, **189**, 357-64.

Rotolo N, Floridi C, Imperatori A, et al (2015). Comparison of cone-beam CT-guided and CT fluoroscopy-guided transthoracic needle biopsy of lung nodules. *Eur Radiol*, 2015.

Schegerer AA, Lechel U, Ritter M, et al (2014). Dose and image quality of cone-beam computed tomography as compared with conventional multislice computed tomography in abdominal imaging. *Invest Radiol*, **49**, 675-84.

Sun YX, Cheng W, Han X, et al (2014). In vivo experimental study on the effects of fluid in increasing the efficiency of radiofrequency ablation. *Asian Pac J Cancer Prev*, **15**, 5799-804.

Wang CH, Wey KC, Mo LR, et al (2015). Current trends and recent advances in diagnosis, therapy, and prevention of hepatocellular carcinoma. *Asian Pac J Cancer Prev*, **16**, 3595-604.

Wang ZJ, Wang MQ, Duan Feng, et al (2013). Clinical application of transcatheter arterial chemoembolization combined with synchronous C-arm Cone-Beam CT guided radiofrequency ablation in treatment of large hepatocellular Carcinoma. *Asian Pacific J Cancer Prev*, **14**, 1649-54.

Xu C, Lv PH, Huang XE, et al (2015). Efficacy of transarterial chemoembolization combined with radiofrequency ablation in treatment of hepatocellular carcinoma. *Asian Pac J Cancer Prev*, **16**, 6159-62.